Micro-/Nanostructured Highly Crystalline Organic Semiconductor Films for Surface-Enhanced Raman Spectroscopy Applications

Mehmet Yilmaz, Mehmet Ozdemir, Hakan Erdogan, Ugur Tamer, Unal Sen, Antonio Facchetti, Hakan Usta,* and Gokhan Demirel**

The utilization of inorganic semiconductors for surface-enhanced Raman spectroscopy (SERS) has attracted enormous interest. However, despite the technological relevance of organic semiconductors for enabling inexpensive, large-area, and flexible devices via solution processing techniques, these π-conjugated systems have never been investigated for SERS applications. Here for the first time, a simple and versatile approach is demonstrated for the fabrication of novel SERS platforms based on micro-/nanostructured 2,7-dioctyl[1]benzothieno[3,2-b][1]benzothiophene (C8-BTBT) thin films via an oblique-angle vapor deposition. The morphology of C8-BTBT thin films is manipulated by varying the deposition angle, thus achieving highly favorable 3D vertically aligned ribbon-like micro-/nanostructures for a 90° deposition angle. By combining C8-BTBT semiconductor films with a nanoscopic thin Au layer, remarkable SERS responses are achieved in terms of enhancement ($\approx 10^8$), stability (>90 d), and reproducibility (RSD < 0.14), indicating the great promise of Au/C8-BTBT films as SERS platforms. Our results demonstrate the first example of an organic semiconductor-based SERS platform with excellent detection characteristics, indicating that π-conjugated organic semiconductors have a great potential for SERS applications.

1. Introduction

Surface-enhanced Raman spectroscopy (SERS) is a powerful and highly sensitive vibrational spectroscopic method, which enables the detection of chemical and biological molecules at very low concentrations. Since its discovery in 1974,[1] intense research efforts have yielded a variety of novel SERS platforms for different applications in the fields of chemistry, physics, medicine, and biology.[2–5] Over the past few decades, the realization of new SERS platforms has been crucial to enhance the detection efficiencies and to understand the effective enhancement mechanisms. In some of these studies, even the limit of a single molecule detection has been accomplished due to the large enhancement factors.[6,7] The common contributors to most of the SERS processes are electromagnetic and chemical enhancement mechanisms.[2,3,5] Although electromagnetic enhancement mechanism results from light amplification by the excitation of localized surface plasmon resonances (LSPRs), chemical enhancement mechanism mainly relies on charge transfer, where the excitation wavelength is resonant with the metal-molecule charge transfer electronic states.[5] Depending on the nature of a particular substrate and analyte, the SERS enhancement may be ascribed to one or both of these mechanisms. Nevertheless, critical drawbacks remain for several SERS systems preventing practical applications, and consequently, the development of new highly sensitive SERS substrates with good stability and reproducibility remains an active scientific and technological research area.

Dr. M. Yilmaz, H. Erdogan, Prof. G. Demirel
Bio-inspired Materials Research Laboratory (BIMREL)
Department of Chemistry
Gazi University
06500 Ankara, Turkey
E-mail: nanobiotechnology@gmail.com
M. Ozdemir, Prof. H. Usta
Department of Materials Science and Nanotechnology Engineering
Abdullah Gül University
38080 Kayseri, Turkey
E-mail: hakan.usta@agu.edu.tr
Prof. U. Tamer
Department of Analytical Chemistry
Faculty of Pharmacy
Gazi University
06330 Ankara, Turkey
Prof. U. Sen
Department of Mechanical Engineering
Abdullah Gül University
38080 Kayseri, Turkey
Prof. A. Facchetti
Polyera Corporation
8045 Lamon Avenue, Skokie
IL 60077, USA
E-mail: afacchetti@polyera.com
Prof. A. Facchetti
Center of Excellence for Advanced Materials Research (CEAMR)
King Abdulaziz University
Jeddah, Saudi Arabia

DOI: 10.1002/adfm.201502151

Among the various SERS-active materials studied to date, semiconductors have recently attracted growing interest due to their unique properties such as tunable absorption and band gap, stable exciton formation, and excitation Bohr radius.[8–13] Over the past decade, numerous semiconductors such as ZnO,[9] TiO_2,[10] lnAs/GaAs,[11] graphene,[12] and CuTe[13] have been reported as alternative SERS substrates. However, their relatively weak enhancements ($\approx 10^2$–10^4) compared to noble and transition metal-based SERS platforms ($\approx 10^4$–10^8) have limited their employment in further SERS-based applications. In order to enhance their response, one effective method is to combine the semiconductor with a thin metallic film having plasmonic property, which has led to enhancement factors up to 10^6–10^8. These studies demonstrated the key role of metal contact on top of the semiconductor film for SERS-based quantitative measurements.[14–16] Despite recent advances with inorganic semiconductors, to the best of our knowledge, the employment of π-conjugated organic semiconductors for SERS applications has never been demonstrated in the literature. This is rather surprising since organic semiconductors exhibit exceptional charge transport/light manipulation properties and excellent contact formation with metals such as Au and Ag in various optoelectronic devices such as organic field-effect transistors (OFETs),[17–29] organic light-emitting diodes (OLEDs),[30] and organic photovoltaics (OPVs).[31–34]. These advances were possible thanks to numerous studies on both the design and synthesis of high-performance π-conjugated structures as well as on semiconductor device fabrication. The design and development of new SERS platforms based on organic semiconductors are technologically attractive considering their facile and low-temperature film deposition also on mechanically flexible plastic substrates and compatibility with low-cost manufacturing/direct-write printing techniques.[35,36] Thus, the compatibility of organic semiconductors with different substrates to fabricate inexpensive, large-area, and flexible devices may further extend the scope of SERS applications. The above considerations prompted us to develop new organic semiconductor-based micro-/nanostructured thin films and to investigate their properties as SERS-active platforms. We envision that, in order to achieve high enhancement factor along with good stability and reproducibility, the molecular semiconductor should display several key properties such as 2D/3D micro-/nanostructured thin-film formation, favorable charge-transport/semiconductor–metal interface and high thermal/electrical stability in the solid state. A molecular semiconductor having these aforementioned properties might be a good candidate to be combined with a metallic thin film for SERS applications.

Here we report, for the first time, a simple and versatile approach for the fabrication of a novel SERS platform based on an organic molecular semiconductor thin film capped with an Au thin layer. To this end, we selected the high-performance *p*-type semiconductor, 2,7-dioctyl[1]benzothieno[3,2-b][1]benzothiophene (C8-BTBT) developed by Takimiya and coworkers[37] due to its exceptional semiconductor properties (hole mobilities up to ≈30–40 $cm^2\ V^{-1}\ s^{-1}$), proper molecular energy levels and good charge injection from Au thin-film electrodes (**Scheme 1**a).[37–39] In addition, the high electrical and thermal stability of C8-BTBT is expected to enhance the stability and robustness of the SERS substrates. The organic

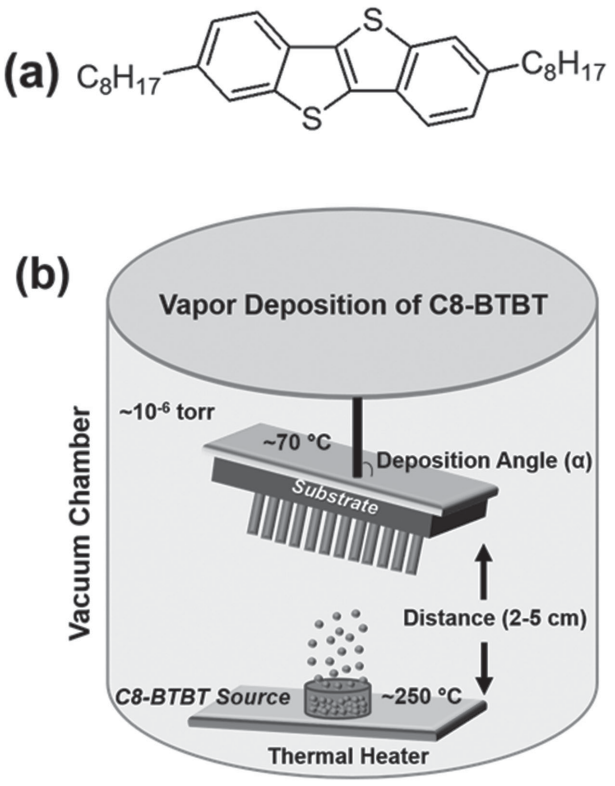

Scheme 1. a) Chemical structure of C8-BTBT and b) schematic representation of the oblique-angle deposition process.

semiconductor film was deposited via an oblique-angle vapor deposition technique, which enables the control of the semiconductor film morphology. Remarkable SERS performances were achieved in terms of enhancement ($\approx 10^8$), stability (>90 d), and reproducibility (RSD < 0.14).

2. Results and Discussion

The synthesis of C8-BTBT was carried out in three steps according to a reported procedure (Figure S1, Supporting Information).[37,40] Due to its good solubility in common organic solvents (e.g., $CHCl_3$, CH_2Cl_2, THF, and toluene), the purification of the final semiconductor was performed by flash column chromatography with silicagel and hexanes as the stationary and mobile phases, respectively. The semiconductor's chemical structure and purity were verified by $^1H/^{13}C$ NMR spectroscopy and elemental analysis (Figure S2, Supporting Information).

Organic semiconductor based micro-/nanostructured thin films were fabricated on silicon substrates via vapor phase deposition of C8-BTBT under high vacuum (1×10^{-6} torr), which enables the deposition of ≈3.0 µm thick semiconductor films (Scheme 1b). Film depositions were performed via an oblique-angle method where 10° and 90° deposition angles (α) were used. For further comparison, solution-processed thin films were also fabricated by spin-coating a C8-BTBT solution in $CHCl_3$ (4 mg mL^{-1}) at 1000 rpm.

The Fourier transform infrared (FTIR) spectrum of C8-BTBT thin films indicates that no chemical changes occur during

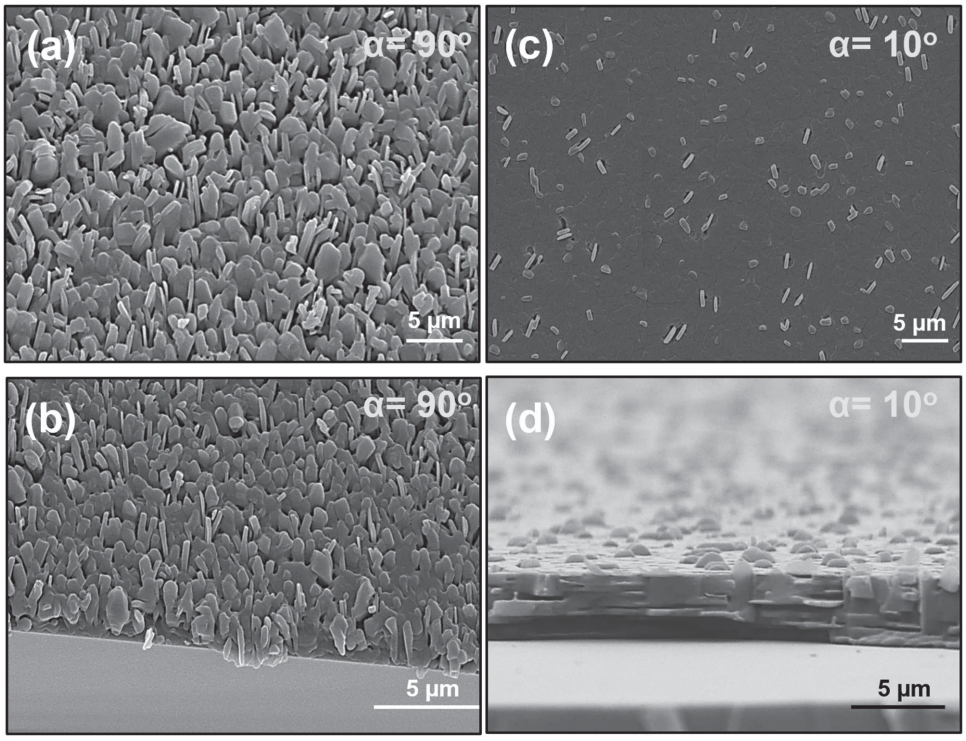

Figure 1. Top-view and cross-sectional SEM images of C8-BTBT films fabricated by vapor deposition at a,b) $\alpha = 90°$ and vapor deposition c,d) at $\alpha = 10°$.

the vapor phase deposition of the semiconductor thin films (Figure S3, Supporting Information), in agreement with the good thermal stability of this material. **Figure 1** displays the top-view and cross-sectional scanning electron microscope (SEM) images of all C8-BTBT films. As shown in Figure 1, the film morphologies are found to dramatically change upon the deposition method and the deposition angle, α. For the semiconductor films deposited by vapor-deposition at $\alpha = 10°$ and by spin-coating, 2D microstructures with highly interconnected plate-like grains are observed (Figure 1d and Figure S4, Supporting Information). A closer look at these films via cross-sectional SEM shows that platelet microstructures with thicknesses of 70–500 nm are stacked on top of each other to adopt a face-on orientation relative the substrate surface. In sharp contrast, when the deposition angle was changed from 10° to 90°, high density arrays of vertically aligned ribbon-like micro-/nanostructures, which are highly favorable for SERS applications,[41,42] were observed (Figure 1a,b). The heights of these edge-on features are 0.8–3.0 μm. Considering that similar π–π stacking interactions between the planar benzothieno[3,2-b]-[1]benzothiophene aromatic cores and van der Waals interactions between lipophilic alkyl chains at the molecular termini are operative during film deposition, the observed morphological differences undoubtedly reflect variations in film-growth mechanisms due to different deposition thermodynamics/kinetics and shadowing effects. For the spin-coated films, the observed highly interconnected 2D plate-like microstructures are most likely due to the ultrafast kinetics of film formation process (<5 s) preventing 3D morphological arrangements in such a short time. Similarly, for vapor-deposited films grown at an angle of 10°, the shadowing effect seems to play a key role compared to $\alpha = 90°$ deposited films. The self-shadowing effect and the high C8-BTBT molecule-molecule affinity result in a 2D film growth with platelets having different thicknesses.[43] Both of these 2D film morphologies indicate a Frank-Van der Merwe growth mode ($\gamma_{\text{semiconductor-film}} + \gamma_{\text{semiconductor-substrate interface}} = \gamma_{\text{substrate}}$), which favors a layer-by-layer 2D film formation on the silicon surface.[44] Out-of-plane X-ray diffraction (XRD) measurements of the semiconductor films deposited at $\alpha = 10°$ exhibits a series of strong sharp reflections up to the third order (001 peak at 3.12°) (Figure S5, Supporting Information). The interlayer distance (*d*-spacing) elucidated from these reflections (28.3 Å) is very close to that of the previously reported spin-coated C8-BTBT films (29.0 Å), and corresponds to the computed molecular length of C8-BTBT with fully extended alkyl chains (all-trans configuration) (28.2 Å, Figure S6a, Supporting Information).[37] In addition, the semiconductor film XRD reflections are assignable to the (001), (002), and (003) peaks in the simulated (random crystallite orientation) powder pattern generated from the single-crystal data (Figure S7, Supporting Information), and the interlayer distance matches well with the *c*-axis length of the crystallographic unit cell (29.1 Å, Figure S6b, Supporting Information).[43] Therefore, it is very likely that the out-of-plane thin-film microstructure is identical to that of the single-crystal along the crystallographic *c*-axis direction and edge-on molecular orientation is favored on the substrate. This is also consistent with the observed layer-by-layer growth (2D film morphology) since an edge-on orientation promotes π–π stacking and van der Waals interactions in the in-plane direction. The BFDH (Bravais, Friedel, Donnay, and Harker) theoretical crystal morphology of C8-BTBT also demonstrates that edge-on molecular arrangement is favorable along the 2D

crystal plane (Figure S8, Supporting Information). On the other hand, vapor-deposited films grown at $\alpha = 90°$ point to the vertical growth of organic nano-/microribbons via an island growth mechanism, which may take place either from the beginning of the film growth process (the Volmer–Weber growth mode, $\gamma_{\text{semiconductor-film}} + \gamma_{\text{semiconductor-substrate interface}} > \gamma_{\text{substrate}}$),[45] or follows an initial 2D wetting layer (the Stranski–Krastanov growth mode). Since the Stranski–Krastanov mechanism of layer-plus-island growth has been previously reported for similarly deposited films of *p*-type semiconductors including metal phthalocyanine derivatives, it is very likely that the present C8-BTBT-based vertical nano-/microribbon formation follows a similar growth mechanism.[46–48] However, we should note that a very detailed study on ultrathin molecular layers of C8-BTBT is needed to fully understand the present vertical growth mechanism. XRD measurement of the 3D C8-BTBT film fabricated at $\alpha = 90°$ exhibits a different set of diffraction peaks up to fifth order (Figure S5a, Supporting Information), with the first one located at 3.94° (*d*-spacing = 22.4 Å). These peaks are assignable to a single phase of (00*l*) reflections revealing that these nano-/microstructures are highly textured. However, none of these peaks can be identified in the simulated XRD powder pattern (Figure S7, Supporting Information), indicating that a considerably different molecular packing occurs in these vertically oriented nano-/microstructures. It is very plausible that this different microstructural ordering observed in $\alpha = 90°$ deposited films is responsible for the 3D morphology formation. Since the *d*-spacing measured for the 90° deposited film is significantly lower than the C8-BTBT molecular length, the semiconductor molecules may be tilted with their long axes at ≈40° from the substrate normal (Figure S6c, Supporting Information). This molecular arrangement would lead to a more effective intermolecular interactions along the vertical direction (enhanced out-of-plane π–π stacking and van der Waals interactions), which ultimately can drive this unique vertical crystal growth.

Figure 2 illustrates a comparison of the UV–vis absorption spectra of C8-BTBT in solution and as thin films. The films fabricated at $\alpha = 10°$ and 90° display a lower bandgap (3.3–3.4 eV) and red-shifted absorption maxima (355 nm) compared to those in solution (3.6 eV, 310 nm). Although the solution spectrum shows the strongest absorption for the 0–2 vibrational peak, and the 0–0 vibrational absorption rises as a shoulder peak, for the thin films, the 0–0 vibrational peak is the strongest. The increased 0–0 intensity relative to the 0–1 and 0–2 transitions and the large red-shifted absorption maxima (≈45 nm) suggest significant J-type aggregate formation. This is consistent with the highly crystalline nature of these thin films, and support the existence of strong intermolecular interactions in the solid state.

Next, we investigated C8-BTBT-based 3D thin films for SERS experiments. However, instead of using single-layer semiconductor films, we utilized a bilayer structure where a thin layer of gold (≈32 nm) covers the C8-BTBT films. In this way, we can combine the plasmonic properties of the metallic layer with the semiconductor chemical enhancement mechanisms via the charge-transfer process. To understand whether the 3D surface morphology of the semiconductor change upon gold deposition, we first performed SEM analysis of the C8-BTBT film capped with the Au layer (Figure S9, Supporting Information), which indicates that the film microstructure is preserved after Au coating. Next, the SERS activity of these films was evaluated by using methylene blue (MB) as the Raman reporter molecule. In a typical sample preparation, a 3 µL MB solution (1×10^{-3} M) was dropped onto the gold-coated C8-BTBT films and the samples left in a hood until dry, which led to coin-shaped MB films of 4 ± 1 mm in size. **Figure 3** shows the MB SERS spectra collected from the gold coated C8-BTBT thin films. For comparison, the spectra obtained from a smooth gold surface having a ≈32 nm thick Au film is also shown in the same figure. All collected spectra are well defined and have acceptable signal-to-noise ratios, consistent with our earlier reports for MB.[41,42] For all cases, the most prominent peaks in the spectra of MB can be summarized as follows: ring stretch (ν(C—C)) at ≈1620 cm^{-1}, symmetric and asymmetric C—N stretches (ν_{sym}(C—N) and ν_{asym}(C—N)) at ≈1395 and ≈1433 cm^{-1}, respectively, and the C—N—C skeletal deformation mode (δ(C—N—C)) at ≈449 cm^{-1}.

Interestingly, gold-coated C8-BTBT films fabricated at $\alpha = 90°$ exhibit a remarkable increment of the SERS signal intensities relative to that of the smooth gold film. On the other hand, although C8-BTBT thin-films deposited at $\alpha = 10°$ does not show any obvious 3D morphology, a dramatic enhancement in the SERS signal is also observed, possibly due to formation of plasmonic hot spots after gold deposition.[49] In order to substantiate this conclusion, we investigated the surface morphology of the gold-coated C8-BTBT film deposited at $\alpha = 10°$. The SEM image reveals that deposited gold on the C8-BTBT

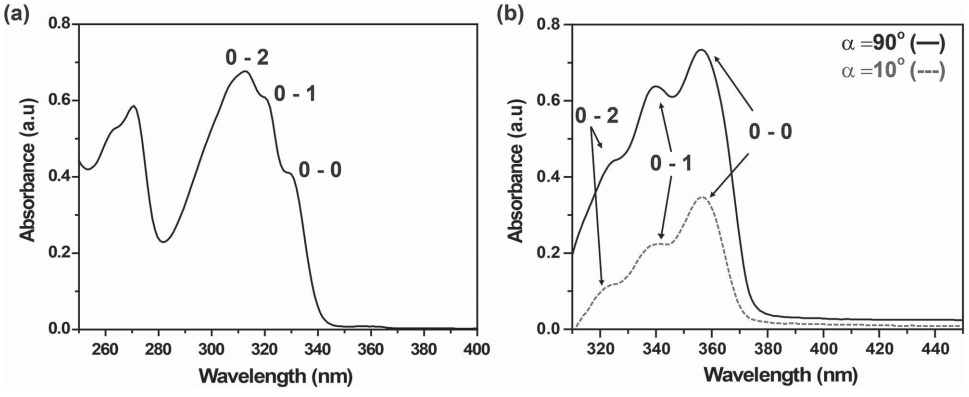

Figure 2. UV–vis spectra of C8-BTBT in a) chloroform solution and b) as vapor deposited thin-films for different deposition angles.

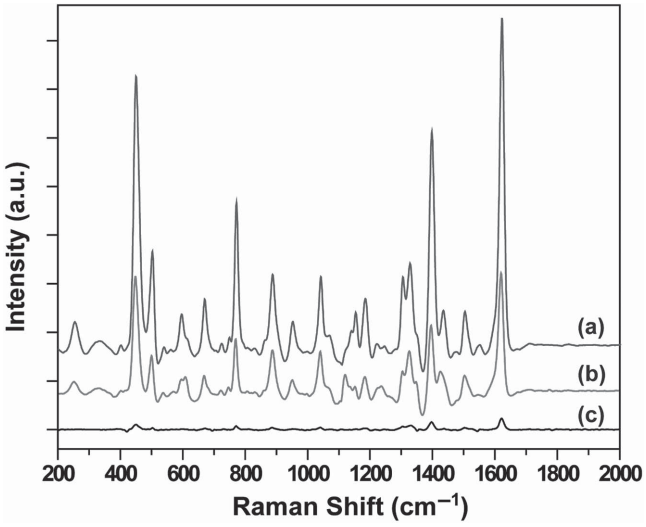

Figure 3. SERS spectra of methylene blue (MB) on Au-coated C8-BTBT films fabricated at a) $\alpha = 90°$ and b) $\alpha = 10°$, and of c) a smooth gold film on silicon.

film forms island-like structures possibly due to dewetting of Au during metal deposition (Figure S10, Supporting Information). The broadened and red-shifted UV–vis spectrum of the Au-coated C8-BTBT film deposited at 10° compared to those deposited at 90° also verifies Au island formation (Figure S11, Supporting Information). Furthermore, we calculated the SERS enhancement factors (EF) to quantify and compare the SERS performances of our samples by applying the following equation and using the MB Raman peak intensity at ≈1620 cm^{-1};

$$\mathrm{EF} = (N_{\mathrm{Bulk}} \times I_{\mathrm{C8\text{-}BTBT}}) / (N_{\mathrm{C8\text{-}BTBT}} \times I_{\mathrm{Bulk}}) \quad (1)$$

where I_{Bulk} and $I_{\mathrm{C8\text{-}BTBT}}$ are the Raman intensities of pure bulk MB and the adsorbed MB on the Au-coated C8-BTBT films, and N_{Bulk} and $N_{\mathrm{C8\text{-}BTBT}}$ are the number of MB molecules for the reference sample and C8-BTBT for different fabrication conditions. Accordingly, the EFs are calculated as 4.7×10^7 for $\alpha = 10°$ and 2.1×10^8 for $\alpha = 90°$.

The impressive SERS signal enhancements may be attributed to different mechanisms. Fundamentally, two main enhancement mechanisms are widely accepted to explain the overall SERS effect: electromagnetic and chemical enhancement mechanisms.[5] Since the surface plasmon resonant frequency of most semiconductors is located in the infrared region,[50] which is far from the 785 nm exciting line in our experiments, electromagnetic contributions to the SERS signal in our system mainly originates from nanostructured or island-like gold films deposited on the C8-BTBT semiconductor film. In the case of C8-BTBT film fabricated at $\alpha = 90°$, a 3D morphology results in the generation of hot spots with an extremely high electric field enhancement as a result of the tip-focusing, cavity resonances and antenna effects.[41,42] This factor is the dominant contributor to the observed high SERS signal enhancement for this particular film. On the other hand, for the C8-BTBT films fabricated at $\alpha = 10°$, island like gold formations, which are very effective to create hot spots as a result of stronger enhancement of the local electromagnetic field by closely placed gold nanostructures, should be the main contributor to the observed electromagnetic enhancement. Note, the enhancement factors achieved in the current organic semiconductor-gold bilayer substrates are significantly higher (>1000×) than those of pristine rough gold films and 3D gold nanorod arrays previously reported through oblique-angle deposition methods (≈10^4–10^5).[42,51] These data demonstrate the key role of the underlying organic semiconductor in the observed high SERS activity of the final substrates. Therefore, in addition to electromagnetic enhancements, micro-/nanoscale charge-transfer processes in the C8-BTBT/gold/MB interfaces may be another important contributor to SERS signal enhancement possibly by magnifying the molecular polarizability.

Two feasible routes for charge transfer may occur upon laser excitation, which are either from C8-BTBT/gold substrate to adsorbed MB molecule or from MB molecule to C8-BTBT/gold substrate. The highest occupied molecular orbital (HOMO) and lowest unoccupied molecular orbital (LUMO) energy levels of C8-BTBT molecule are found to be −5.5 eV and −2.2 eV, respectively, based on the cyclic voltammetry and optical absorption data.[37] The work function of the gold is −5.1 eV.[52] In addition, the HOMO and LUMO energy levels of MB, which is used as the Raman reporter in our work, are −4.7 and −3.6 eV, respectively.[53,54]

The laser light used in this study has a wavelength of 785 nm (1.58 eV), which is sufficient to enable electron transfer between C8-BTBT/gold/MB interfaces. Based on the interfaces and the energy levels in our system, the two feasible charge transfers may involve the following steps:[55] in the first route (**Scheme 2**a), an electron occupying the ground state of MB is first excited from HOMO to an energy level above LUMO by the incident laser light. Then, the excited electron transfers quickly to a matching energy level of the C8-BTBT/gold layers through resonant tunneling. The underlying C8-BTBT semiconductor may help the electron transfer via formation of metal–organic interfacial states. Subsequently, the electron is transferred back to the ground state of MB emitting a Raman photon while leaving the MB molecule at some vibrational state. The second route (Scheme 2b) involves charge transfer from the substrate to MB, with an electron in the valence band of the gold/substrate is first excited to the conduction band of gold upon laser excitation. At this point, a hole is also generated in the valence band of the gold film, which can be further delocalized and stabilized with the underlying *p*-channel C8-BTBT semiconductor. This would further accelerate the separation of the electron-hole pair and facilitate the charge transfer mechanism. Then, the excited electron is quickly transferred from the substrate to the matching energy level above the LUMO of MB molecule through resonant tunneling, which eventually transits back to the C8-BTBT/gold substrate and recombine with the hole. During this process, a vibrational quantum of energy transfers to the MB vibrational level and a Raman photon is radiated. It is noteworthy that similar charge-transfer mechanisms were previously proposed for inorganic semiconductor-based SERS systems.[55] Although more detailed experiments and theoretical modeling are needed to fully rationalize these processes, the observed SERS enhancement plausibly reflects a complex interplay of these

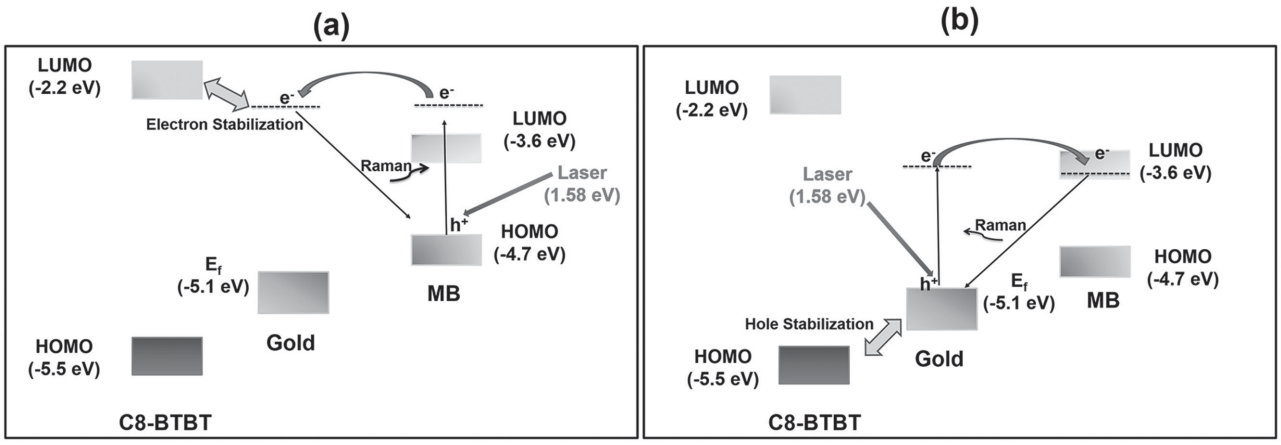

Scheme 2. Schematic representations for possible charge-transfer mechanisms (a and b) between MB and the Au/C8-BTBT film.

aforementioned electromagnetic enhancement and charge transfer mechanisms.

The poor reproducibility of SERS signals is one of the major drawbacks of Raman studies,[56,57] and it should be addressed to prove that a system may be suitable for SERS applications. To demonstrate the reproducibility of our SERS platform, we collected SERS spectra from 30 randomly selected spots on the C8-BTBT thin films under identical experimental conditions. From the data of **Figure 4**, it is clear that for all runs, the Raman spectra are highly reproducible. We calculated the relative standard deviation (RSD) values to clarify and quantify the reproducibility of the same spectra given in Figure 4. **Table 1** summarizes the RSD results in intensity changes of different Raman peaks. All RSD values are below 0.14, which indicates an excellent reproducibility across the entire area of the SERS platform.

Finally, we tested the stability in ambient conditions of our SERS platform by analyzing the Raman peak intensities and positions over time. As shown in **Figure 5**, for the first 30–60 d of aging, no change in the Raman spectra was observed. However, after 90 d of storing, the MB SERS signal was found to exhibit a small intensity reduction of ≈15% without any shift in the peak position, probably due to humidity variations. However, our results clearly prove the robust environmental stability of the present organic semiconductor-based SERS structure. It is likely that the stability of our platform may be further improved by proper passivation or encapsulation, since these procedures are typical for achieving stable organic semiconductor-based optoelectronic devices.[58]

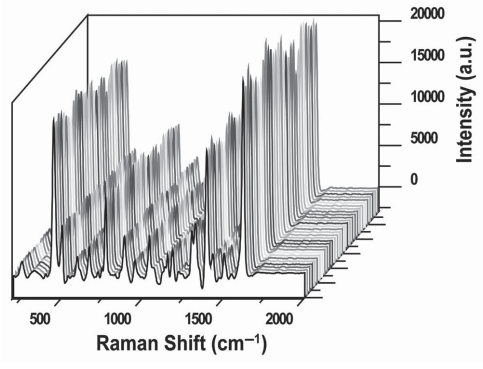

Figure 4. Reproducibility of SERS spectra of MB collected on randomly selected 30 spots of the Au/C8-BTBT platforms.

3. Conclusion

In conclusion, we demonstrated, for the first time, a simple and versatile approach for the fabrication of micro-/nanostructured C8-BTBT films through an oblique-angle vapor deposition technique and tested them as active platforms for SERS applications. For a 90° deposition angle, vertically aligned 3D ribbon-like crystalline micro-/nanostructured C8-BTBT thin films are fabricated, whereas smooth and highly interconnected 2D thin films having stacked platelet microstructures are obtained at $\alpha = 10°$. By coating these C8-BTBT films with a thin layer of gold, remarkable SERS performances in terms of enhancement, stability, and reproducibility were achieved. Our results clearly show that π-conjugated semiconductor thin-films, when combined with metallic films, represent a new promising entry for the fabrication of SERS-active substrates, and they should be studied more in future SERS applications.

4. Experimental Section

Materials and Methods: All reagents were purchased from commercial sources and used without further purification unless otherwise noted. Conventional Schlenk techniques were used, and reactions were carried out under N_2 unless otherwise noted. NMR spectra were recorded on a Bruker 400 spectrometer (^{1}H, 400 MHz). Elemental analyses were performed by Midwest Microlab, LLC.

Table 1. RSD values for the major peaks of the SERS spectrum for 30 MB spots.

Peak position [cm^{-1}]	1620	1395	1303	1183	770	449
RSD value	0.11	0.13	0.09	0.14	0.10	0.10

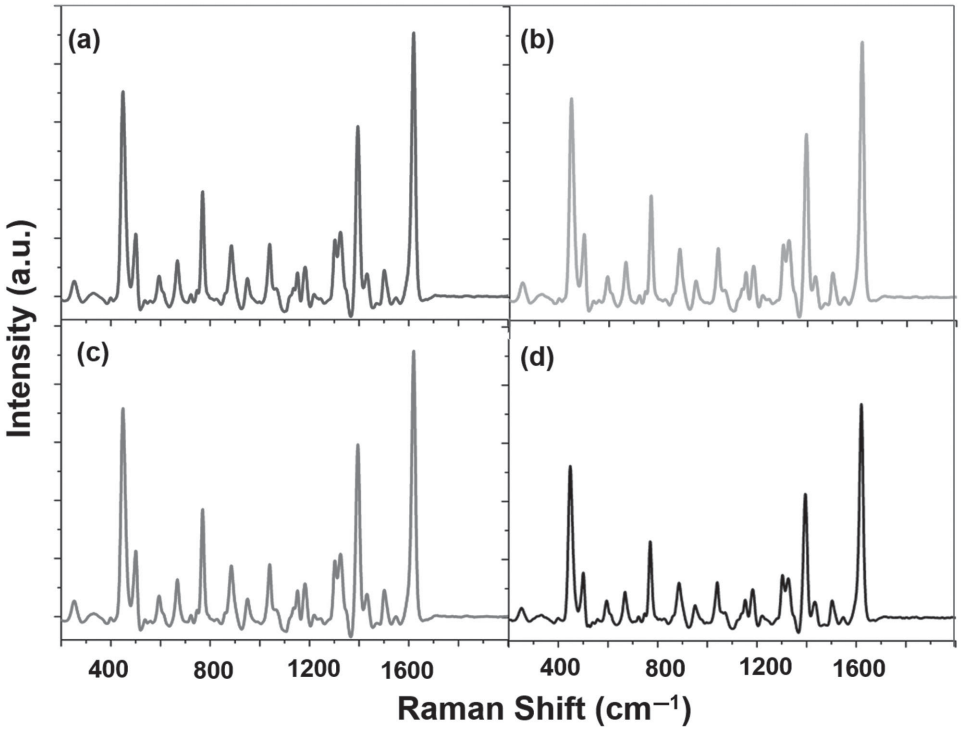

Figure 5. SERS spectra of MB obtained from the a) freshly fabricated sample and stored for b) 30, c) 60, and d) 90 d in ambient air.

Sythesis and Characterization: The synthesis of benzothieno[3,2-b]-[1]benzothiophene (BTBT, **1**) was performed according to the reported procedure.[40]

Synthesis of ([1]Benzothienopheno[3,2-b]benzothienophene-2,7-diyl)bis-(octan-1-one) (2): To a solution of [1]benzothieno[3,2-b][1]benzothiophene (1.0 g, 4.16mmol) in 50 mL of anhydrous dichloromethane, $AlCl_3$ (3.07 g, 23 mmol) was added at –10 °C under nitrogen. The resulting mixture was stirred at –10 °C for 30 min, and then octanoylchloride (3.41 g, 21 mmol) was added dropwise. The reaction mixture was stirred at –10 °C for 1 h, and then at room temperature for 2 d. The reaction mixture was poured into water to yield a white precipitate. The precipitate was collected by vacuum filtration, and washed with water and methanol, respectively, to give **2** (1.3 g, 64% yield) as a white crystalline solid. This compound was directly used in the next step without any further purification. ^{1}H NMR δ 8.56 (d, J = 1.3 Hz, 2H), 8.06 (dd, J = 8.0, 1.3 Hz, 2H), 7.95 (d, J = 8.0 Hz, 2H), 3.07 (t, J = 7.0 Hz, 4H), 1.75–1.83 (m, 4H), 1.20–1.52 (m,16H), 0.90 (t, J = 7.2Hz, 6H).

Synthesis of ([1]Benzothienopheno[3,2-b]benzothienophene-2,7-diyl)-bis(octan-1-one) (C8-BTBT): To a solution of ([1]benzothienopheno[3,2-b]-benzothienophene-2,7-diyl)bis(octan-1-one) (2, 1.0 g, 2.03 mmol) and potassium hydroxide (626 mg, 11.2 mmol) in diethyleneglycol (50 mL) was added hydrazinehydrate (3.2 mL, 51.75 mmol) under nitrogen, and the resulting solution was heated to 110 °C for 1 h and then further heated at 210 °C for 5 h. After cooling to room temperature, a white precipitate formed, which was filtered and washed with water and methanol to yield a white crude solid. The crude compound was next chromatographed on silica, eluting with hexanes to yield C8-BTBT as a white crystalline solid (0.66 g, 70% yield). ^{1}H NMR δ 7.76 (d, J = 8.0 Hz, 2H), 7.71 (d, J = 1.0 Hz, 2H), 7.27 (dd, J = 8.0 Hz,1.0 Hz, 2H), 2.76 (t, J = 8.0 Hz, 4H), 1.71 (m, 4H), 1.26–1.36 (m, 20H), 0.89 (t, J = 6.8 Hz, 6H); ^{13}C NMR δ 143.2, 140.5, 132.7, 131.1, 124.9, 122.9, 121.2, 36.2, 31.9, 32.0, 29.2, 29.1, 28.8, 22.5, 13.9; Anal. Calcd for $C_{30}H_{40}S_2$: C, 77.53; H, 8.67. Found: C, 77.20; H, 8.50.

Fabrication of SERS Platforms Based on C8-BTBT Thin Films: The silicon wafers with (001) crystallographic orientations and 1–10 Ω cm resistivity were first cut (1.5 × 1.5 cm^2) and washed with deionized water, acetone, and piranha solution consecutively. To eliminate any contaminants, pre-cleaned wafers were then treated with oxygen plasma at low pressure (0.2 mbar) for 30 min before C8-BTBT deposition. In a typical experiment, C8-BTBT powder (10–20 mg) was placed onto tungsten boat and evaporated at about 250 °C under fixed base pressure (1 ± 0.2 × 10^{-6} torr) in a physical vapor deposition (PVD) system (NANOVAK HV, Ankara, Turkey) for varying deposition times (1–5 min) on cleaned silicon wafers. The distance between C8-BTBT source and substrate was also altered ranging from 1 to 5 cm. A simple handmade device was utilized to manipulate deposition angle. After fabrication of C8-BTBT films, a thin layer gold (32 nm) was deposited in the same PVD system at the similar base pressure. For comparison of SERS performances, smooth gold films having 32 nm of Au thickness were also fabricated in the same manner. The tilt angle (θ) was calculated from the computed molecular length (l) and the film d-spacing (d) determined from the film XRD ($d = l \times \cos\theta$).

SERS Measurements: For all Raman studies, a Delta Nu Examiner Raman Microscopy system equipped with a 785 nm laser source, a motorized microscope stage sample holder, and a cooled charge-coupled device (CCD) detector was used in the range of 200–2000 cm^{-1}. Experimental parameters were as follows: 20× objective, 3 μm spot size, 30 s acquisition time, 150 mW laser power and baseline correction was performed for all measurements. To evaluate the SERS enhancement, an aqueous solution of MB in different concentrations was prepared and 3 μL of this solution was dropped onto the gold-coated C8-BTBT thin films and kept in a hood until dry. The drying procedure created coin-shaped Raman samples of size of 4 ± 1 mm onto the substrates. For each sample, at least ten Raman spectra were collected from the different spots of substrate to determine the reproducibility and homogeneity.

Computational Methodology: Geometry optimizations and electronic structure calculations for the gas-phase neutral states of C8-BTBT were carried out by density functional theory (DFT) calculations at the B3LYP/6-31G** level of theory using Spartan PC (Spartan '08, Version 1.0.0, Wavefunction, Inc.)

Supporting Information

Supporting Information is available from the Wiley Online Library or from the author.

Acknowledgements

The authors thank Prof. M. O. Guler for his support with the synthesis of C8-BTBT semiconductor. G.D. acknowledges support from the Turkish Academy of Sciences, Distinguished Young Scientist Award (TUBA-GEBIP). H.U. acknowledges support from The Science Academy, Young Scientist Award (Bilim Akademisi-BAGEP). A.F. also thanks KAU for support.

Received: May 26, 2015
Revised: July 21, 2015
Published online: August 11, 2015

[1] M. Fleischman, P. J. Hendra, A. J. McQuillan, *Chem. Phys. Lett.* **1974**, *26*, 163.
[2] Y. S. Huh, A. J. Chung, D. Erickson, *Microfluid. Nanofluid.* **2009**, *6*, 285.
[3] G. McNay, D. Eustace, W. E. Smith, K. Faulds, D. Graham, *Appl. Spectrosc.* **2011**, *65*, 825.
[4] B. Sharma, R. R. Frontiera, A. I. Henry, E. Ringe, R. P. Van Duyne, *Mater. Today* **2012**, *15*, 16.
[5] P. L. Stiles, J. A. Dieringer, N. C. Shah, R. P. Van Duyne, *Annu. Rev. Anal. Chem.* **2008**, *1*, 601.
[6] K. Kneipp, Y. Wang, H. Kneipp, L. T. Perelman, I. Itzkan, R. R. Dasari, M. S. Feld, *Phys. Rev. Lett.* **1997**, *78*, 1667.
[7] S. Nie, S. R. Emory, *Science* **1997**, *275*, 1102.
[8] J. R. Lombardi, R. L. Birke, *J. Phys. Chem. C* **2014**, *118*, 11120.
[9] Z. Mao, W. Song, L. Chen, W. Ji, X. Xue, W. Ruan, Z. Li, H. Mao, S. Ma, J. R. Lombardi, *J. Phys. Chem. C* **2011**, *115*, 18378.
[10] D. Maznichenko, K. Venkatakrishnan, B. Tan, *J. Phys. Chem. C* **2012**, *117*, 578.
[11] L. G. Quagliano, *J. Am. Chem. Soc.* **2004**, *126*, 7393.
[12] W. Xu, X. Ling, J. Xiao, M. S. Dresselhaus, J. Kong, H. Xu, Z. Liu, J. Zhang, *Proc. Natl. Acad. Sci. USA* **2012**, *109*, 9281.
[13] W. Li, R. Zamani, P. Rivera Gil, B. Pelaz, M. Ibáñez, D. Cadavid, A. Shavel, R. A. Alvarez-Puebla, W. J. Parak, J. Arbiol, *J. Am. Chem. Soc.* **2013**, *135*, 7098.
[14] W. Ji, Y. Kitahama, X. Han, X. Xue, Y. Ozaki, B. Zhao, *J. Phys. Chem. C* **2012**, *116*, 24829.
[15] X. Li, G. Chen, L. Yang, Z. Jin, J. Liu, *Adv. Funct. Mater.* **2010**, *20*, 2815.
[16] C. Wen, F. Liao, S. Liu, Y. Zhao, Z. Kang, X. Zhang, M. Shao, *Chem. Commun.* **2013**, *49*, 3049.
[17] H. Usta, W. C. Sheets, M. Denti, G. Generali, R. Capelli, S. Lu, X. Yu, M. Muccini, A. Facchetti, *Chem. Mater.* **2014**, *26*, 6542.
[18] H. Usta, M. D. Yilmaz, A. J. Avestro, D. Boudinet, M. Denti, W. Zhao, J. F. Stoddart, A. Facchetti, *Adv. Mater.* **2013**, *25*, 4327.
[19] M. Caironi, T. D. Anthopoulos, Y. Y. Noh, J. Zaumseil, *Adv. Mater.* **2013**, *25*, 4208.
[20] M. C. Chen, S. Vegiraju, C. M. Huang, P. Y. Huang, K. Prabakaran, S. L. Yau, W. C. Chen, W. T. Peng, I. Chao, C. Kim, *J. Mater. Chem. C* **2014**, *2*, 8892.
[21] L. Zhang, A. Fonari, Y. Liu, A. L. M. Hoyt, H. Lee, D. Granger, S. Parkin, T. P. Russell, J. E. Anthony, J. L. Brédas, *J. Am. Chem. Soc.* **2014**, *136*, 9248.
[22] B. Vercelli, M. Pasini, A. Berlin, J. Casado, J. T. López Navarrete, R. P. Ortiz, G. Zotti, *J. Phys. Chem. C* **2014**, *118*, 3984.
[23] S. R. Walter, J. Youn, J. D. Emery, S. Kewalramani, J. W. Hennek, M. J. Bedzyk, A. Facchetti, T. J. Marks, F. M. Geiger, *J. Am. Chem. Soc.* **2012**, *134*, 11726.
[24] Q. Wei, Y. Lin, E. R. Anderson, A. L. Briseno, S. P. Gido, J. J. Watkins, *ACS Nano* **2012**, *6*, 1188.
[25] K. Takimiya, I. Osaka, M. Nakano, *Chem. Mater.* **2013**, *26*, 587.
[26] R. Matsidik, H. Komber, A. Luzio, M. Caironi, M. Sommer, *J. Am. Chem. Soc.* **2015**, *137*, 6705.
[27] Y. Zhang, H. Dong, Q. Tang, S. Ferdous, F. Liu, S. C. Mannsfeld, W. Hu, A. L. Briseno, *J. Am. Chem. Soc.* **2010**, *132*, 11580.
[28] J. Y. Hu, M. Nakano, I. Osaka, K. Takimiya, *J. Mater. Chem. C* **2015**, *3*, 4244.
[29] D. Natali, M. Caironi, *Adv. Mater.* **2012**, *24*, 1357.
[30] S. R. Forrest, *Nature* **2004**, *428*, 911.
[31] B. Kippelen, J. L. Brédas, *Energy Environ. Sci.* **2009**, *2*, 251.
[32] A. Riaño, P. M. Burrezo, M. J. Mancheño, A. Timalsina, J. Smith, A. Facchetti, T. Marks, J. L. Navarrete, J. Segura, J. Casado, *J. Mater. Chem. C* **2014**, *2*, 6376.
[33] H. Lee, E. Puodziukynaite, Y. Zhang, J. C. Stephenson, L. J. Richter, D. A. Fischer, D. M. DeLongchamp, T. Emrick, A. L. Briseno, *J. Am. Chem. Soc.* **2015**, *137*, 540.
[34] P. Kumaresan, S. Vegiraju, Y. Ezhumalai, S. L. Yau, C. Kim, W. H. Lee, M. C. Chen, *Polymers* **2014**, *6*, 2645.
[35] B. Kang, W. H. Lee, K. Cho, *ACS Appl. Mater. Interfaces* **2013**, *5*, 2302.
[36] S. Mandal, G. Dell'Erba, A. Luzio, S. G. Bucella, A. Perinot, A. Calloni, G. Berti, G. Bussetti, L. Duò, A. Facchetti, *Org. Electron.* **2015**, *20*, 132.
[37] H. Ebata, T. Izawa, E. Miyazaki, K. Takimiya, M. Ikeda, H. Kuwabara, T. Yui, *J. Am. Chem. Soc.* **2007**, *129*, 15732.
[38] H. Minemawari, T. Yamada, H. Matsui, J. Tsutsumi, S. Haas, R. Chiba, R. Kumai, T. Hasegawa, *Nature.* **2011**, *475*, 364.
[39] Y. Yuan, G. Giri, A. L. Ayzner, A. P. Zoombelt, S. C. Mannsfeld, J. Chen, D. Nordlund, M. F. Toney, J. Huang, Z. Bao, *Nat. Commun.* **2014**, *5*, 3005.
[40] B. I. Košata, V. Kozmik, J. I. Svoboda, V. Novotná, P. E. Vaněk, M. Glogarová, *Liq. Cryst.* **2003**, *30*, 603.
[41] M. S. Akin, M. Yilmaz, E. Babur, B. Ozdemir, U. Tamer, G. Demirel, *J. Mater. Chem. B* **2014**, *2*, 4894.
[42] M. Yilmaz, E. Senlik, E. Biskin, M. S. Yavuz, U. Tamer, G. Demirel, *Phys. Chem. Chem. Phys.* **2014**, *16*, 5563.
[43] T. Izawa, E. Miyazaki, K. Takimiya, *Adv. Mater.* **2008**, *20*, 3388.
[44] M. A. Herman, W. Richter, H. Sitter, *Epitaxy: Physical Principles and Technical Implementation*, Springer Science & Business Media, Berlin–Heidelberg, Germany **2004**.
[45] B. Mutaftschiev, *The Atomistic Nature of Crystal Growth*, Springer Science & Business Media, Berlin–Heidelberg, Germany **2001**.
[46] Y. Zhang, Y. Diao, H. Lee, T. J. Mirabito, R. W. Johnson, E. Puodziukynaite, J. John, K. R. Carter, T. Emrick, S. C. B. Mannsfeld, A. L. Briseno, *Nano Lett.* **2014**, *14*, 5547.
[47] A. Wise, Y. Zhang, J. Fan, F. Wudl, A. L. Briseno, M. Barnes, *Phys. Chem. Chem. Phys.* **2014**, *16*, 15825.
[48] G. Demirel, U. Tamer, *Nanotechnology* **2012**, *23*, 225604.
[49] B. N. Khlebtsov, V. A. Khanadeev, E. V. Panfilova, D. N. Bratashov, N. G. Khlebtsov, *ACS Appl. Mater. Interfaces* **2015**, *7*, 6518.
[50] L. Yang, X. Jiang, W. Ruan, B. Zhao, W. Xu, J. R. Lombardi, *J. Phys. Chem. C* **2008**, *112*, 20095.
[51] P. M. Tessier, O. D. Velev, A. T. Kalambur, J. F. Rabolt, A. M. Lenhoff, E. W. Kaler, *J. Am. Chem. Soc.* **2000**, *122*, 9554.
[52] H. B. Michaelson, *J. Appl. Phys.* **1977**, *48*, 4729.
[53] J. S. Lee, K. H. You, C. B. Park, *Adv. Mater.* **2012**, *24*, 1084.
[54] Y. Ocak, M. Kulakci, T. Kılıçoğlu, R. Turan, K. Akkılıç, *Synth. Met.* **2009**, *159*, 1603.
[55] X. Wang, W. Shi, G. She, L. Mu, *J. Am. Chem. Soc.* **2011**, *133*, 16518.
[56] D. K. Lim, K. S. Jeon, J. H. Hwang, H. Kim, S. Kwon, Y. D. Suh, J. M. Nam, *Nat. Nanotechnol.* **2011**, *6*, 452.
[57] X. Liu, Y. Shao, Y. Tang, K. F. Yao, *Sci. Rep.* **2014**, *4*, 5835.
[58] H. J. Yang, M. H. Yi, T. Ahn, *Mol. Cryst. Liq. Cryst.* **2014**, *600*, 138.